

The capacity loss of a RCC building under mainshock-aftershock seismic sequences

Chang-Hai Zhai^{*1,2,3}, Zhi Zheng^{4a}, Shuang Li^{1,2,3a} and Xiaolan Pan^{4a}

¹School of Civil Engineering, Harbin Institute of Technology, Harbin 150090, China

²Key Lab of Structures Dynamic Behavior and Control (Harbin Institute of Technology), Ministry of Education, Heilongjiang, Harbin, 150090, China.

³Key Lab of Smart Prevention and Mitigation of Civil Engineering Disasters of the Ministry of Industry and Information Technology, Harbin Institute of Technology, Harbin 150090, China.

⁴College of Architecture and Civil Engineering, Taiyuan University of Technology, Taiyuan 030024, China

(Received December 29, 2016, Revised April 17, 2018, Accepted June 26, 2018)

Abstract. Reinforced concrete containment (RCC) building has long been considered as the last barrier for keeping the radiation from leaking into the environment. It is important to quantify the performance of these structures and facilities considering extreme conditions. However, the preceding research on evaluating nuclear power plant (NPP) structures, particularly considering mainshock-aftershock seismic sequences, is deficient. Therefore, this manuscript serves to investigate the seismic fragility of a typical RCC building subjected to mainshock-aftershock seismic sequences. The implementation of the fragility assessment has been performed based on the incremental dynamic analysis (IDA) method. A lumped mass RCC model considering the tri-linear skeleton curve and the maximum point-oriented hysteretic rule is employed for IDA analyses. The results indicate that the seismic capacity of the RCC building would be overestimated without taking into account the mainshock-aftershock effects. It is also found that the seismic capacity of the RCC building decreases with the increase of the relative intensity of aftershock ground motions to mainshock ground motions. In addition, the effects of artificial mainshock-aftershock ground motions generated from the repeated and randomized approaches and the polarity of the aftershock with respect to the mainshock on the evaluation of the RCC are also researched, respectively.

Keywords: reinforced concrete containment building; mainshock-aftershock effects; fragility assessment; HCLPF capacity; IDA

1. Introduction

Currently, an increasing number of studies on seismic performance of buildings affected by mainshock-aftershock sequence-type ground motions or multiple ground motions have been conducted because multiple ground motions may be seen as extreme seismic conditions. Of all these studies, many investigations have been conducted to incorporate the effects of aftershocks on reinforced concrete structures (Alliard and Leger 2008, Hatzigeorgiou and Liolios 2010, Efraimiadou *et al.* 2013, Faisal *et al.* 2013, Zhang *et al.* 2013, Han *et al.* 2014, Shin *et al.* 2014, Raghunandan *et al.* 2015, Tesfamariam *et al.* 2015, Zhai *et al.* 2015). These studies show that aftershocks may have a significant disadvantageous influence on the seismic performance of structures. As the last barrier for keeping the radiation from leaking into the environment, reinforced concrete containment (RCC) building has long been neglected under extreme conditions, particularly for mainshock-aftershock seismic sequences. Hence, this manuscript serves to investigate the seismic performance of a typical RCC

building subjected to mainshock-aftershock seismic sequences.

To date, seismic fragility analysis has been widely used to evaluate different types of structures including moment frames (Guneyisi and Sahin 2014, Lee and Kim 2015), masonry buildings (Ranjbaran and Hosseini 2014), bridges (Olmos *et al.* 2002), and etc. According to EPRI (2003) and American Nuclear Society standard (ANS 2007), seismic fragility analysis of a structure, system, and component (SSC) of a nuclear power plant (NPP) is an integral step of seismic probabilistic safety assessments (SPSA). Hence, developing a new fragility curve of the SSC of a NPP more accurately and reasonably would better enrich the seismic risk assessment of the NPP. Moreover, seismic capacity of the NPP determined through the fragility analysis will be helpful for seismic design and evaluation of NPP structures and facilities.

During the past thirty years, great progress has been made by researchers to improve the seismic evaluation of NPP structures and facilities. Early in 1983, the Nuclear Regulatory Commission and the nuclear industry jointly developed a procedures guide (USNRC 1983) for the performance of probabilistic risk assessments (PRA) of nuclear power plants. After one year, Kennedy and Ravindra (1984) provided guidelines for NPP structures and facilities on appropriate techniques, available sources of

*Corresponding author, Professor
E-mail: zch-hit@hit.edu.cn

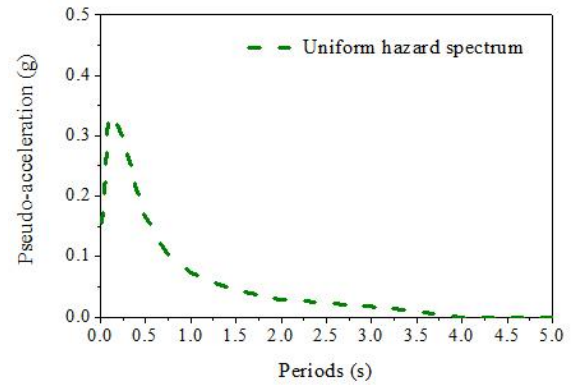
^aPh.D.

data, representative results, and key contributors to seismic risk based on the experience gained in conducting fragility evaluation for about a dozen PRA studies. After that, a great number of studies on seismic evaluation of NPP structures and facilities had been conducted. Some researchers established complicated numerical models to investigate the seismic fragility of NPP structures and facilities (Vermaut *et al.* 1998, De Grandis *et al.* 2009, Nakamura *et al.* 2010, Viallet *et al.* 2010). Other researchers mainly employed simple lumped-mass stick models to quantify the seismic fragility of NPP structures and facilities (Ghiocel *et al.* 1998, Takeda *et al.* 1998, Ozaki *et al.* 1998, Cho and Joe 2005, Choi *et al.* 2006, Zentner 2010, Huang *et al.* 2011a, b). In addition, fragility parameters about nuclear structures and components provided by guidelines or codes had also been used for fragility evaluation of NPP structures (Ellingwood 1998, Park *et al.* 1998, Kim *et al.* 1998). Nevertheless, one limitation of the above analyses is that none of those studies focused on assessing the seismic performance of nuclear structures or facilities considering extreme seismic conditions, particularly for mainshock-aftershock seismic sequences. The capacity loss due to aftershock ground motions needs to be determined in a probabilistic sense in order that the reasonable seismic design and evaluation of NPP structures and facilities can be facilitated. Besides, to the authors' best knowledge, all the seismic design codes or guidelines related to nuclear structures in the world are based on the single 'design earthquake' without taking into account the influence of mainshock-aftershock sequences. Consequently, it is necessary and urgent to investigate the effect of mainshock-aftershock sequence-type ground motions on the seismic evaluation of nuclear structures.

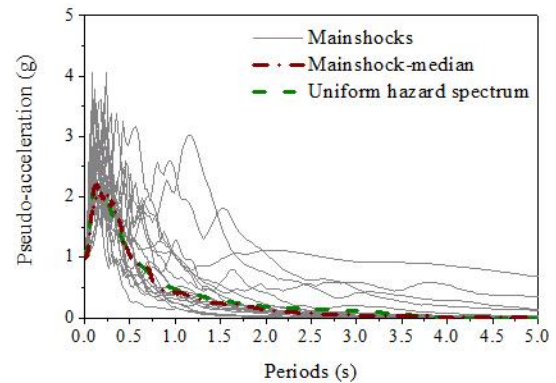
Moreover, aftershock ground motions with different relative intensities would induce different additional structural damage (Hatzigeorgiou and Beskos 2009, Goda and Taylor 2012, Hatzigeorgiou 2010a, b, Ruiz-García and Negrete-Manriquez 2011, Zhai *et al.* 2014). It is significant to consider different levels of the relative intensity of the aftershock ground motion when investigating the seismic performance of structures under mainshock-aftershock sequence-type ground motions. Therefore, through using the repeated approach and the randomized approach to generate sequential ground motions, this manuscript also introduces the effect of aftershock ground motions with different intensity levels for the seismic evaluation of the RCC building. Additionally, the effect of the polarity of the aftershock with respect to the mainshock on seismic evaluation of the RCC building is also considered and investigated.

2. Mainshock-aftershock ground motions

Ground motion records that are used for evaluating the seismic performance of structures need to be selected carefully to reflect regional dominant earthquake scenarios. Probabilistic seismic hazard analysis (PSHA) accounts for uncertainties related to earthquake occurrence, source rupture, wave propagation, and site effects by integrating hazard contributions over all scenarios. Based on a site



(a) Target response spectrum



(b) Response spectra for as-recorded mainshocks

Fig. 1 Target response spectrum and response spectra for as-recorded mainshocks

evaluation report conducted by a nuclear company, the uniform hazard spectrum with a probability of exceedance of 10^{-4} in 60 years is obtained (Fig. 1(a)).

The strong ground motion database that has been used here consists of twenty real seismic sequences from the PEER-NGA database for worldwide shallow crustal earthquakes and the complete list of these earthquakes appears in Table 1. Specifically, 96 seismic sequence records compatible with the following criteria are downloaded firstly from the PEER-NGA database. These criteria are: (a) magnitudes of most mainshocks are close to 6.0; (b) accelerograms are recorded by stations which are located in free field; (c) peak ground accelerations (*PGAs*) of mainshocks are equal to or greater than 0.1g; (d) accelerograms are recorded on rock or stiff soil. Moreover, the twenty records have been selected by identifying the set best reproducing the target response spectrum through automatically combining the records downloaded from the strong motion databases based on a Monte Carlo random selection method. The elastic spectra (viscous damping ratio $\xi=5\%$; *PGAs* of mainshocks are scaled to 1.0 g) for mainshocks and the target spectrum are presented in Fig. 1(b). It can be seen that the mean response spectrum has a good fitting with respect to the target spectrum by scaling all the selected records to the same *PGA*. Notice that while the mean magnitude of as-recorded aftershocks ($M_s=5.56$) is lower than that of as-recorded mainshocks ($M_s=6.21$), the mean *PGA* for aftershocks is almost equal to that for mainshocks.

Table 1 Detailed information of selected seismic sequences

No.	Ground motion	Station	Comp.	V_{s30} (m/s)	Mainshock			Aftershock			PGA_{as}/PGA_{ms}
					Time	Mag. (M_s)	PGA	Time	Mag. (M_s)	PGA	
1	Whittier	SM	270	379.4	10/01/87	6	0.128	10/04/87	5.3	0.156	1.22
2	Whittier	SM	360	379.4	10/01/87	6	0.204	10/04/87	5.3	0.212	1.04
3	Whittier	AFS	180	550	10/01/87	6	0.333	10/04/87	5.3	0.174	0.52
4	Whittier	AFS	270	550	10/01/87	6	0.414	10/04/87	5.3	0.178	0.43
5	Mammoth Lakes	MLHS	270	346.8	05/25/80	6.06	0.321	05/25/80	5.69	0.39	1.21
6	Mammoth Lakes	MLHS	360	346.8	05/25/80	6.06	0.239	05/25/80	5.69	0.441	1.85
7	Mammoth Lakes	CL(con)	180	472.2	05/31/80	4.8	0.196	06/11/80	4.85	0.191	0.97
8	Mammoth Lakes	CL(con)	270	472.2	05/31/80	4.8	0.206	06/11/80	4.85	0.183	0.89
9	Irpinia	RIV	000	574.9	11/23/80	6.9	0.106	11/23/80	6.2	0.099	0.93
10	Irpinia	RIV	270	574.9	11/23/80	6.9	0.104	11/23/80	6.2	0.096	0.92
11	Coalinga	SB	000	617.4	07/22/83	5.77	0.141	07/25/83	5.21	0.152	1.08
12	Coalinga	SB	090	617.4	07/22/83	5.77	0.127	07/25/83	5.21	0.23	1.81
13	Whittier	AEC	000	375.2	10/01/87	6	0.299	10/04/87	5.3	0.264	0.88
14	Whittier	AEC	090	375.2	10/01/87	6	0.151	10/04/87	5.3	0.199	1.32
15	Irpinia	Calitri	000	455.9	11/23/80	6.9	0.132	11/23/80	6.2	0.177	1.34
16	Irpinia	Calitri	270	455.9	11/23/80	6.9	0.176	11/23/80	6.2	0.165	0.94
17	Chi-Chi	TCU075	E	573	09/20/99	7.62	0.33	09/20/99	6.2	0.22	0.67
18	Chi-Chi	TCU075	N	573	09/20/99	7.62	0.26	09/20/99	6.2	0.15	0.58
19	Whittier	MWCSS	000	680.4	10/01/87	6	0.123	10/04/87	5.3	0.158	1.28
20	Whittier	MWCSS	090	680.4	10/01/87	6	0.186	10/04/87	5.3	0.142	0.76
Mean						6.21	0.209		5.56	0.199	1.01

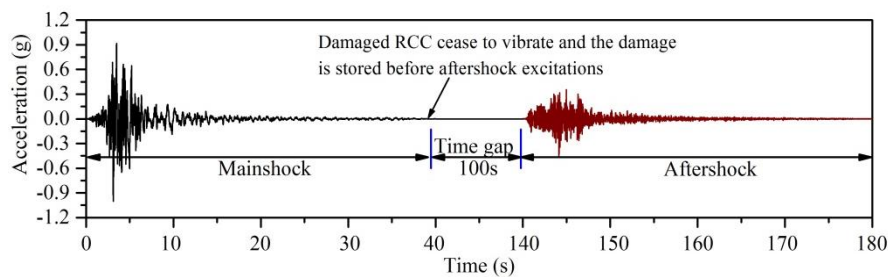


Fig. 2 A scenario mainshock-aftershock acceleration time history

Each of the aforementioned sequential motions has been separated into a single ground motion where a 100s gap is applied between two consecutive seismic events. This gap has zero acceleration ordinates and is sufficient to allow the structure to cease moving after the previous event. It is evident that, when the RCC sustains damage at the end of the mainshock, aftershocks would lead to increased damage for the mainshock-damaged RCC, as shown in Fig. 2.

3. Modelling of the RCC building

3.1 Characteristics of the RCC building

A typical RCC building, which houses the nuclear reactor and safety-related equipment, is selected to conduct the analysis in this paper. Fig. 3(a) shows the cutaway view of the RCC building and reinforcement details. The RCC

building consists of a base slab, a perimeter wall, and an upper dome. The inside diameter of the cylinder is 37.796 m and its height is 43.830 m. The inside radius of the dome is 18.898 m and the total height of the containment building is 63.094 m. The wall thickness in the cylinder part is 1.067 m and in the dome 0.762 m. The density, Poisson's ratio, elastic modulus, compressive strength, and tensile strength of the concrete for the containment are 2400 kg/m³, 0.2, 33000 MPa, 32.4 MPa, and 2.67 MPa, respectively. The yield force for the steel is 350 MPa.

3.2 Analysis model

Compared to the fine three-dimensional finite element model, the simple lumped-mass stick model is both effective and efficient for a large number of dynamic time history analysis of the RCC. Besides, the simple lumped-mass stick model was also demonstrated to reflect the

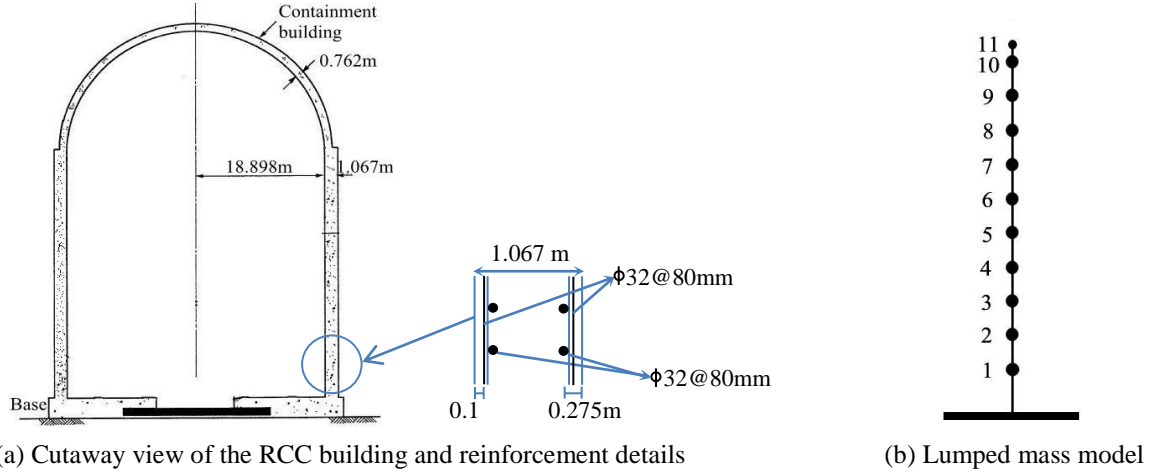


Fig. 3 The RCC building and its analytical model

Table 2 Properties of the lumped mass model for the RCC building (Concrete modulus $E_c=3.30 \times 10^4$ MPa, Steel modulus $E_s=2.0 \times 10^5$ MPa)

No.	Height (m)	M_g (kN)	Area (mm^2)	Shear area (mm^2)	Moment of inertia (mm^4)
base	0	88960.0			
1	7.163	20460.8	130064256	65032128	2.41667E+16
2	13.350	18681.6	130064256	65032128	2.41667E+16
3	19.446	18681.6	130064256	65032128	2.41667E+16
4	25.542	18681.6	130064256	65032128	2.41667E+16
5	31.638	18681.6	130064256	65032128	2.41667E+16
6	37.734	18681.6	130064256	65032128	2.41667E+16
7	43.830	20505.28	130064256	65032128	2.41667E+16
8	50.383	13432.96	91974010	46451520	1.63989E+16
9	56.205	10986.56	91974010	46451520	1.29465E+16
10	60.503	9429.76	91974010	46451520	6.90478E+15
11	63.094	845.12	91974010	46451520	1.72619E+15

mechanical behavior of the RCC by the preceding studies (Cho and Joe 2005, Choi *et al.* 2006, Zentner 2010, Huang *et al.* 2011a, b). Hence, a simple lumped mass model is developed using the finite element software OpenSees (Mazzoni *et al.* 2004). Fig. 3(b) shows the lumped mass model for the RCC building. The detailed information of the lumped mass model appears in Table 2.

In order to accurately predict the seismic response of the RCC building subjected to strong earthquakes, the nonlinear behavior of the lumped mass model must be determined. Since the Electric Power Joint Research (EPJR) program (Park and Hofmayer 1994) determined the restoring force characteristics for the reactor building based on a large number of experimental and analytical research, the nonlinear behavior for the RCC model proposed in the program is employed in the following analyses. In this scheme, flexural deformation and the shear deformation are separated from each other, with hysteresis loops determined for each of them independently. Specifically, the tri-linear approximations shown in Figs. 4(a)-(b) are used for the shear and the bending behavior of the lumped mass model, respectively. The turning points for the shear and bending stress-strain relationships are determined based on the EPJR

method, as shown in Eqs. (1)-(5).

In the EPJR method, for both the box wall and the cylindrical wall, the shear stress and shear strain at the first turning point are determined by the following formula

$$\tau_1 = \sqrt{\sqrt{F_c} (\sqrt{F_c} + \sigma_v)} \quad \text{and} \quad \gamma_1 = \tau_1 / G \quad (1)$$

where G is the shear modulus of elasticity of the concrete, F_c is the concrete compression strength, σ_v is the axial compression stress in the longitudinal direction.

According to the EPJR scheme, the shear stress and the corresponding shear strain at the second turning point are determined as follows by using the values at the first turning point

$$\tau_2 = 1.35\tau_1 \quad \text{and} \quad \gamma_2 = 3\gamma_1 \quad (2)$$

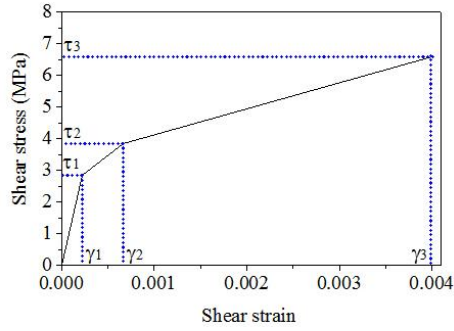
The shear stress and shear strain at the terminating point are determined as follows

$$\left\{ \begin{array}{l} \text{when } \tau_s < 4.5\sqrt{F_c} \quad \tau_3 = \left(1 - \frac{\tau_s}{4.5\sqrt{F_c}} \right) \tau_0 + \tau_s \\ \tau_0 = \left(3 - 1.8 \frac{M}{QD} \right) \sqrt{F_c} \quad \text{and} \\ \tau_s = \frac{P_v + P_h}{2} \sigma_y + \frac{\sigma_v + \sigma_h}{2} \\ \text{when } \tau_s \geq 4.5\sqrt{F_c} \quad \tau_3 = 4.5\sqrt{F_c} \\ \gamma_3 = 0.004 \end{array} \right. \quad (3)$$

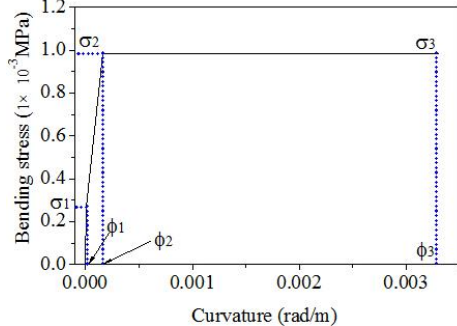
where σ_h is the axial compression stress in the transverse direction, σ_y is the reinforcing bar yield stress, D is the outer diameter in the case of a cylindrical wall, P_v and P_h are longitudinal and transverse reinforcing bar ratio, respectively, M and Q are bending moments and shear force at the bottom of the structure, respectively.

For both the box wall and the cylindrical wall, the bending stress and bending curvature at the first turning point are determined by the following formula

$$\sigma_1 = 1.2\sqrt{F_c} + \frac{N}{A_e} \quad \text{and} \quad \phi_1 = \sigma_1 \cdot Z_e / K_e \quad (4)$$



(a) shear behavior



(b) bending behavior

Fig. 4 Tri-linear skeleton curves

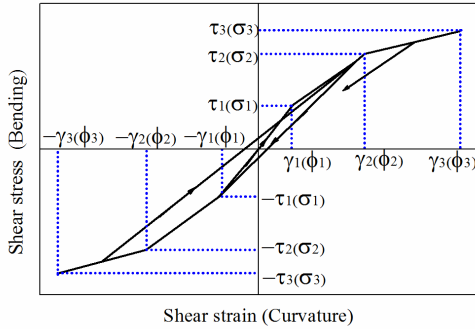


Fig. 5 Hysteretic rule of the maximum point-oriented model

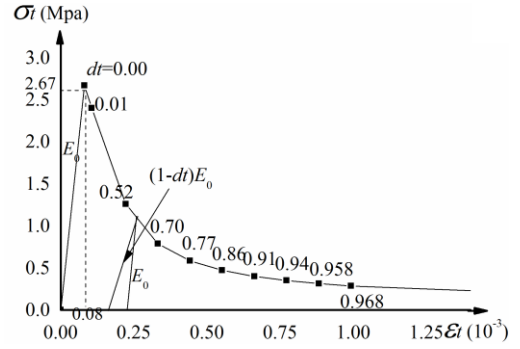
where N is the axial force, A_e is the effective cross-sectional area with reinforcing bars taken into consideration, Z_e is the effective section modulus, K_e is the elastic bending stiffness.

On the other hand, σ_2 and ϕ_2 are taken as the flexural moment and curvature when the tensile reinforcing bar yields. In addition, σ_3 is calculated by using the total plastic formula, and the curvature corresponding to σ_3 is calculated as follows

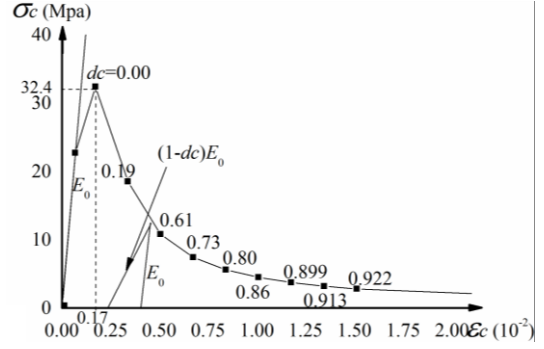
$$\begin{cases} \text{when } \phi_3 < 20\phi_2 & \phi_3 = 0.004 / \chi_{nu} \\ \text{when } \phi_3 \geq 20\phi_2 & \phi_3 = 20\phi_2 \end{cases} \quad (5)$$

where χ_{nu} is the distance from the extreme compression fiber to the centroid of the full-plastic cross-section.

To perform the elasto-plastic seismic response analysis, based on the tri-linear skeleton curve, the maximum point-oriented model is used as the hysteretic rule for the repeated loading and unloading processes (Park and Hofmayer 1994). Fig. 5 shows the hysteretic rule of the maximum



(a) Tensile behavior



(b) Compressive behavior

Fig. 6 Assumed constitutive behavior of concrete

point-oriented model.

The nonlinearBeamColumn element object in OpenSees computer package, considering the spread of plasticity along the element, is assigned to the lumped mass model. The SectionAggregator object which groups previously-defined shear and flexure behaviors into a single section force-deformation model is adopted to construct the nonlinearBeamColumn element object. The self-developed hysteretic rule for the maximum point-oriented model is included in the OpenSees platform for the following earthquake response analysis.

3.3 Verification of the analysis model

For the verification of the lumped mass model, a three-dimensional finite element model for the RCC building is first established using the finite element software ABAQUS. As the thickness of the cylinder of the containment building is less than one-tenth of the radius of the cylinder, the cylinder is modeled using shell elements into which rebars are embedded. The semi-circle dome and the base are modeled using shell elements and 8-node solid elements, respectively. It should be noted that rebars are completely bonded to the concrete. A constitutive concrete model with characteristics of damaged plasticity proposed by Lubliner *et al.* (1989) and modified by Lee and Fenves (1998) is used here for the containment concrete. The plastic deformation and stiffness degradation constitute the uniaxial strength functions for this model. Therefore, the stiffness degradation, expressed by the tensile damage dt and the compressive damage dc , is described as shown in Fig. 6. A bilinear restoring force with the second gradient 1/100 of the initial stiffness is considered for the rebars. Fig.



Fig. 7 Three-dimensional finite element model for the RCC building

Table 3 Modal analysis results for the three-dimensional model and the lumped mass model

Mode	Three-dimensional model (along X component)		Lumped mass model	
	Frequency	Effective mass coefficient	Frequency	Effective mass coefficient
1	5.368 Hz	70.4 %	5.291 Hz	72.6 %
2	15.637 Hz	20.4 %	15.625 Hz	21.3 %
3	30.590 Hz	4.1 %	29.411 Hz	4.5 %

7 displays the three-dimensional finite element model.

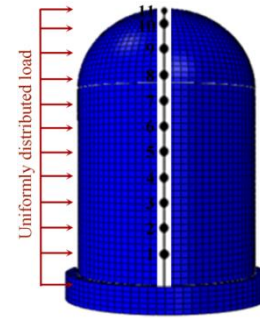
A comparison of modal analysis results between the lumped mass model and the three-dimensional model is carried out to demonstrate the availability of the simple lumped mass model. The modal analysis results are presented in Table 3. The fundamental frequencies of the RCC building estimated by the three-dimensional finite element model and the lumped mass model are 5.368 Hz and 5.291 Hz, respectively. The second and third frequencies also show a good agreement. More importantly, the effective mass coefficient between both models has a high similarity for each mode. Therefore, the lumped mass model can be used to approximately represent the three-dimensional finite element model for the dynamic time history analysis.

For verification of the lumped mass model in the case of nonlinear behavior, the static pushover analysis with uniformly distributed load for both the lumped mass model and the three-dimensional model is performed, as shown in Fig. 8(a). The comparison of the pushover curves between the above two models is given in Fig. 8(b). It can be seen that the pushover curves for the two models have a good agreement, indicating that the lumped model is an ideal alternative to the three-dimensional model for the following seismic response analyses. It is also found from the pushover curve that the softening initiation occurs when the top displacement reaches 13.2 mm while the crushing initiation is caused with the top displacement increasing to 149 mm.

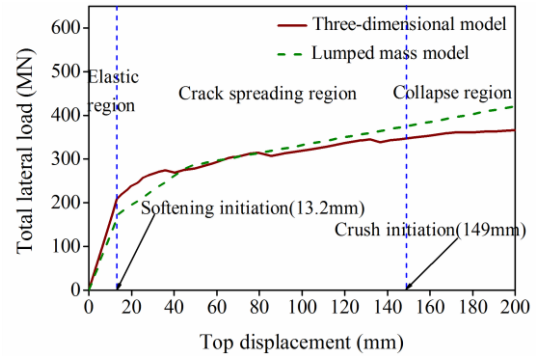
4. Fragility calculation

4.1 Fragility calculation method

The fragility analysis defines a set of curves that express



(a) Schematic diagram for pushover analysis



(b) The pushover analysis results

Fig. 8 The comparison of pushover analysis between three-dimensional model and lumped mass model

a probability of failure versus ground motion levels at different confidence levels. In other words, the seismic fragility of a structure represents probabilistically the capability of a ground motion to cause structural damage. Since the fragility calculation method proposed by Kennedy and Ravindra (1984) is commonly used to evaluate NPP structures and facilities, the method is employed for the fragility evaluation of the RCC building in this study. The failure probability of a structure $P_f(a)$ at any non-exceedance probability level Q can be obtained from the Eq. (6)

$$P_f(a) = \Phi \left(\frac{\ln(a / A_m) + \beta_U \Phi^{-1}(Q)}{\beta_R} \right) \quad (6)$$

where $\Phi(\cdot)$ is the standard Gaussian cumulative distribution function, a is a given PGA , $\Phi^{-1}(\cdot)$ is the inverse of the standard Gaussian cumulative distribution function, A_m is the median ground acceleration capacity, and β_R and β_U represent the randomness of the ground acceleration capacity due to earthquakes and the uncertainty of the model, respectively.

In this study, the median ground acceleration capacity A_m and the β_R for mainshocks and seismic sequences are calculated in sects. 4.2-4.3. The β_U value equal to 0.32 recommended by Ozaki *et al.* (1998), Choi *et al.* (2006) is utilized to represent the uncertainty of the model.

4.2 Incremental dynamic analysis of the RCC building

Incremental dynamic analysis (IDA) is a parametric analysis method that is useful for estimating structural

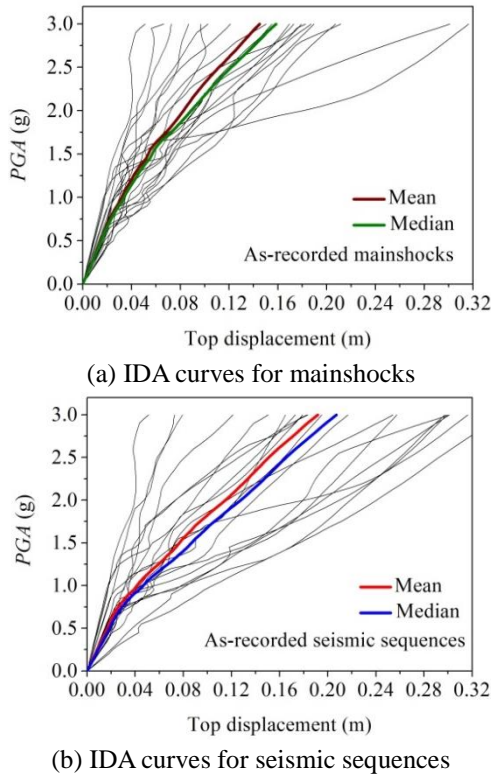


Fig. 9 IDA curves for as-recorded mainshocks and seismic sequences

performance under several ground motions. The method is discussed comprehensively by Vamvatsikos and Cornell (Vamvatsikos and Cornell 2002). It mainly involves producing one or more curves of damage measure (DM) versus intensity measure (IM) under the effect of scaled ground motions as a result of several non-linear dynamic analyses. Since the maximum top displacement and PGA are the most widely used damage measure and intensity measure for evaluating NPP structures, the maximum top displacement is assumed as the damage indicator and PGA is selected as the ground motion intensity measure in this study. Each ground motion is scaled monotonically with respect to PGA of mainshock ground motions. The corresponding aftershocks multiply the same scale factor as the mainshocks. An increment of 0.02 g (sometimes 0.002 g) in PGA is selected in order to capture the cracking and crushing capacities of the structure with a reasonable sensitivity. The OpenSees computer package (Mazzoni *et al.* 2004) is used for the non-linear dynamic analysis, and the maximum top displacement is recorded at the end of each run. Figs. 9(a)-(b) show the IDA curves generated for the RCC building excited by the as-recorded mainshocks and seismic sequences, respectively. The IDA curves show the record-to-record variability between different ground motions. Further observing the IDA curves, it is clear that while each ground motion is scaled up to 3.0 g, the tangent slope of most IDA curves has never degraded too much because the applied skeleton curves for the lumped mass model in Fig. 4 have no strength degradation. The mean and median IDA curves for mainshocks and seismic sequences are computed and also displayed in Fig. 9. It can be found

from the figure that the mean and median IDA curves show a good agreement for each IDA analysis result.

4.3 Median seismic capacity of the RCC building

The definition of structural capacity or performance level plays a significant role in the construction of fragility curves. Ideally, the capacity model for buildings should be developed based on the previous seismic performance and from experimental data. Due to the lack of experimental data, capacity values for cracking and crushing states are determined using the analysis result.

The first performance level, i.e., cracking state, is identified by the attainment of the yield displacement at which the structure initiates yielding. From the pushover curve in Fig. 8(b), it is found that the structure enters the tensile softening stage when the maximum top displacement reaches 13.2 mm. Hence, the maximum top displacement of 13.2 mm is adopted as the cracking state for the RCC.

When the structure reaches its crushing capacity, practically, an increase in intensity measure produces an infinite increase in damage measure. To determine the crushing capacity of the structure, ground motion is scaled up step by step. The second performance level, i.e., crushing state, is determined by the top displacement at which the maximum top displacement of the RCC reaches 149 mm, as shown in the pushover curve in Fig. 8(b). It should be noted that the approach for determining the crushing limit in this study is, in effect, a DM -based rule. That is when the structural response increases beyond a certain value, the structural model is assumed to be in the limit-state. Compared with the DM -based rule, although the IM -based rule is a better alternative for determining the collapse limit (Vamvatsikos and Cornell 2002), it is not appropriate in this study. Due to a large amount of reinforcing bars embedded in the RCC building, the total strength of the containment wall including concrete and rebars is expected to increase even after cracking, which can be confirmed by the previous experimental data and the proposed skeleton curve (Furukawa *et al.* 1987). Consequently, the dynamic instability (or the last point on the IDA curve that is smaller than the 20% of the initial tangent slope of the IDA curve) could hardly occur under earthquake excitations, i.e., the collapse limit could not be determined using the IM -based rule.

Then, the seismic capacity values for both cracking and crushing states for the RCC building are obtained. The maximum likelihood method is adopted to obtain the median ground acceleration capacity A_m and β_R , as shown in Eq. (7). The obtained parameters (A_m and β_R) of the lognormal curves for the as-recorded mainshocks and seismic sequences are summarized in Table 4.

$$\text{Likelihood} = \left(\prod_{i=1}^m \phi \left(\frac{\ln(A_i / A_m)}{\beta_R} \right) \right) \left(1 - \phi \left(\frac{\ln(A_{\max} / A_m)}{\beta_R} \right) \right)^{n-m} \quad (7)$$

Where Π denotes a product over i values from 1 to m , A_m is the median ground acceleration capacity, A_i is the ground acceleration capacity for i th ground motion, A_{\max} is the maximum A_i that causes the failure of the structure, β_R represents the randomness of the acceleration capacity due

Table 4 Parameters of the lognormal distribution for as-recorded ground motions

	Cracking state		Crushing state	
	A_m	β_R	A_m	β_R
Mainshocks	0.724	0.273	2.809	0.180
Seismic sequences	0.638	0.396	2.316	0.333

to earthquakes, n is the total number of selected ground motions and m is the number of ground motions that causes the failure of the structure.

4.4 Fragility curves subjected to as-recorded ground motions

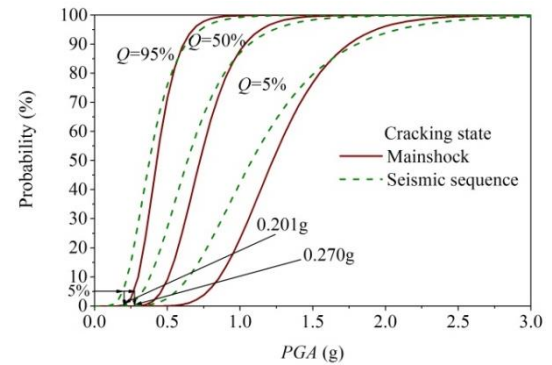
The as-recorded seismic sequences in sect. 2 are employed to investigate the effect of aftershocks on seismic evaluation of the RCC building. After calculating the fragility parameters (A_m and β_R) corresponding to each damage state, the fragility points for a given PGA can be obtained. Figs. 10(a)-(b) show the fragility curves of the RCC building for the as-recorded mainshocks and seismic sequences. A realistic seismic capacity of NPP structures and equipment in the seismic probabilistic risk analysis (SPRA) can also be expressed by the high confidence of low probability of failure (HCLPF) capacity. The HCLPF capacity in the SPRA is defined mathematically as 95% confidence of less than 5% probability of failure, which is generally used as an index to represent the seismic capacity of the structure and equipment in a NPP (Campbell *et al.* 1998). Hence, the calculated HCLPF capacity values are also displayed in Fig. 10.

In Fig. 10, the fragility curves for the as-recorded mainshock-aftershock sequences shift to the left of the curves for the as-recorded mainshocks in most ground motion intensity levels, meaning with a higher probability of cracking or crushing. The HCLPF capacity of the RCC building is 0.270 g for the cracking state under mainshocks while there is a noticeable reduction for the value under seismic sequences, decreasing to 0.201 g and reducing by 25.6%. Similarly, for the crushing state, the HCLPF capacity of the RCC building is 1.228 g under mainshocks while the value for seismic sequences has only 0.794 g, with a loss of 35.3% crushing capacity in comparison with only mainshocks. The obtained results indicate that HCLPF capacities estimated by only mainshocks could be considerably overestimated in comparison with mainshock-aftershock seismic sequences and the effect of aftershocks must be considered for the seismic evaluation of NPP structures.

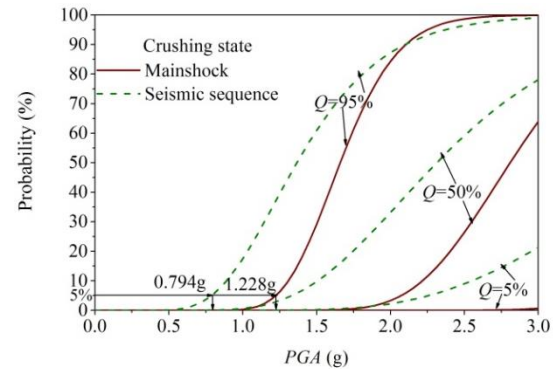
5. Sensitivity analysis for earthquake characteristics to seismic fragility

5.1 Effects of artificial mainshock-aftershock ground motions using repeated approach

It should be noted that most of the previous studies have



(a) Cracking state



(b) Crushing state

Fig. 10 Fragility curves of the RCC for the as-recorded mainshocks and seismic sequences

developed investigations on the effect of aftershocks on the response of structures employing artificial seismic sequences (Li and Ellingwood 2007, Hatzigeorgiou and Beskos 2009, Hatzigeorgiou 2010, Hatzigeorgiou and Liolios 2010). Most studies show that artificial seismic sequences generated from the repeated or randomized approach could consistently increase peak and permanent displacement demands from the mainshocks. Consequently, artificial seismic sequences have the potential to increase the failure probability of the structure while lower the HCLPF capacity. In order to facilitate the seismic design and evaluation of the RCC building under mainshock-aftershocks, it is of interest and necessity to investigate the level of overestimation in the failure probability of the RCC building for artificial seismic sequences. For this purpose, artificial seismic sequences are generated by repeating the as-recorded mainshock as the aftershock (i.e., repeated approach).

To investigate the effect of aftershock ground motions with different relative intensities on the seismic performance of structures, PGA_{as}/PGA_{ms} , being the ratio between peak ground acceleration of aftershock ground motion (PGA_{as}) and that of mainshock ground motion (PGA_{ms}), is defined as the relative intensity of aftershock ground motion. It can be seen from the as-recorded seismic sequences in sect. 2 that the mean PGA for aftershocks is almost equal to that for mainshocks. Therefore, in this study, by scaling the aftershock ground motions, six different levels of relative intensity (i.e. $PGA_{as}/PGA_{ms}=0.5, 0.6, 0.7, 0.8, 0.9$ and 1.0) are considered for each

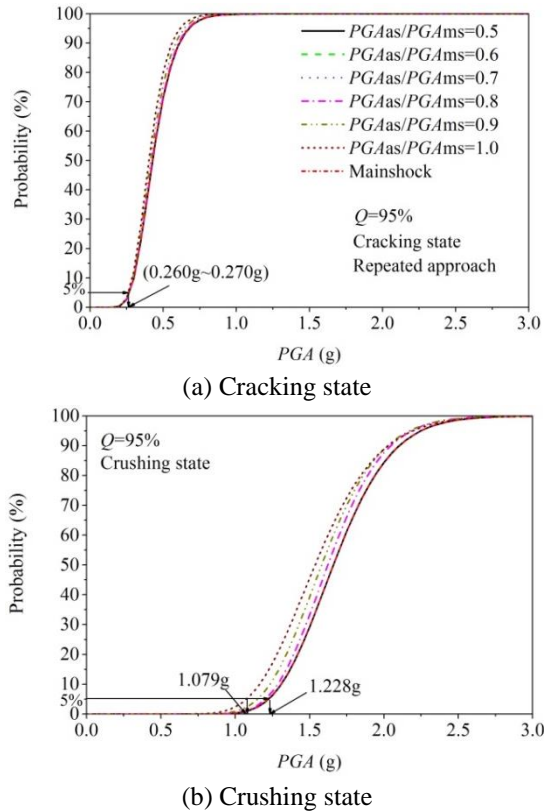


Fig. 11 Fragility curves of the RCC for mainshocks and seismic sequences (repeated approach)

mainshock-aftershock ground motion. As a consequence, 120 (20 mainshocks and 6 relative intensities of aftershocks) artificial sequential ground motions are generated for the fragility analysis of the RCC model.

Based on the IDA results, the fragility curves of the RCC model are derived and the HCLPF capacities are computed in terms of PGA . Fig. 11 illustrates the fragility curves including cracking and crushing states for both mainshocks and seismic sequences with different PGA_{as}/PGA_{ms} values. In Fig. 11(a), the fragility curves for seismic sequences with different PGA_{as}/PGA_{ms} values almost overlap the curves for only mainshocks, indicating that artificial mainshock-aftershocks using the repeated approach have negligible influence on the cracking probability of the RCC model. However, as the building subjects to mainshock-aftershocks with larger PGA_{as}/PGA_{ms} values, it becomes increasingly fragile for the crushing state, as is indicated by the leftward shift of the fragility curves.

For the RCC model in this study, the HCLPF capacities corresponding to cracking and crushing states for all the considered PGA_{as}/PGA_{ms} values are also displayed in Fig. 11. For the cracking state, the HCLPF capacity of the RCC has 0.270 g for only mainshocks and 0.260 g when the relative intensity of aftershock ground motions increases to 1, with negligible difference between mainshocks and seismic sequences. However, for the crushing state, as the level of relative intensity of aftershock ground motions increases, the HCLPF capacity of the RCC subjected to seismic sequences reduces more significantly in comparison

with mainshocks. Specifically, if PGA_{as}/PGA_{ms} is equal to 0.5, 0.6, 0.7, 0.8, 0.9 and 1, respectively, the HCLPF capacity corresponding to the crushing state is 1.228g, 1.228 g, 1.228 g, 1.206 g, 1.156 g and 1.079 g, reducing by 0 %, 0 %, 0 %, 1.8 %, 5.9 % and 12.1 % in comparison with only mainshocks. The above results show that while the RCC building experiences two same ground motions consecutively, the capacity loss of the RCC building would be triggered by repeated sequences, particularly for the crushing state.

5.2 Effects of artificial mainshock-aftershock ground motions using randomized approach

The as-recorded mainshocks and corresponding aftershocks have different frequency content and seismic sequences generated using the repeated approach are not realistic. Hence, the synthesized sequences are generated by seeding the recorded ground motions using the randomized approach. Here, the as-recorded mainshocks in Table 1 are used to generate randomized sequences. For example, one mainshock ground motion in Table 1 is randomly selected as the artificial mainshock and another mainshock is used as the corresponding artificial aftershock. In this part, 400 artificial sequences are generated using the 20 as-recorded mainshocks. The relative intensity of aftershock ground motions is also considered in this part. Fig. 12 compares the fragility curves between randomized seismic sequences and mainshocks. It can be clearly seen that the RCC model has a higher probability of cracking or crushing when subjected to randomized seismic sequences in comparison with only mainshocks. For the HCLPF capacity and the cracking state, the value is 0.270 g under only mainshocks while the value decreases to 0.249 g under artificial seismic sequences with the PGA_{as}/PGA_{ms} value being 1.0, reducing by 7.8 %. It is also noted that the HCLPF capacity for the crushing state reduces from 1.228 g under only mainshocks to 0.879 g under artificial seismic sequences with the PGA_{as}/PGA_{ms} value of 1, with a loss of 28.4 % crushing capacity in comparison with mainshocks.

All the calculated HCLPF capacities for as-recorded and artificial sequential ground motions are summarized in Table 5. From Table 5, for the case of PGA_{as}/PGA_{ms} equal to 0.5, artificial seismic sequences generated from the repeated approach and randomized approach would not lead to lower HCLPF capacities. With the increase of relative intensity of aftershock ground motions, the HCLPF capacities determined by randomized seismic sequences are reduced more significantly than those of repeated seismic sequences, which is probably due to different frequency content between mainshocks and aftershocks. After comparing HCLPF capacities determined by as-recorded seismic sequences and artificial seismic sequences with the PGA_{as}/PGA_{ms} value equal to 1.0, it is clear that as-recorded sequential ground motions result in the lowest HCLPF capacities for the RCC building while repeated seismic sequences are the least conservative. The recommendation for fragility analysis of the RCC building can be given as follows: compared to repeated seismic sequences, randomized seismic sequences are more reasonable because of introduced aftershocks with different frequency content

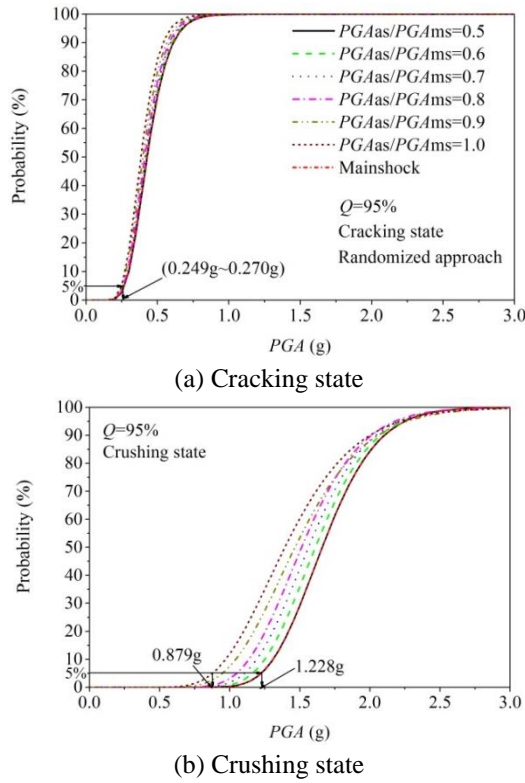


Fig. 12 Fragility curves of the RCC for mainshocks and seismic sequences (randomized approach)

Table 5 HCLPF capacities estimated using as-recorded and artificial sequential ground motions

HCLPF capacity	PGA_{as}/PGA_{ms}	Only mainshocks	As-recorded sequences	Repeated sequences	Randomized sequences
Cracking	0.5			0.270 g	0.270 g
	0.6			0.270 g	0.270 g
	0.7	0.270 g	0.201 g	0.270 g	0.260 g
	0.8			0.270 g	0.258 g
	0.9			0.265 g	0.255 g
	1.0			0.260 g	0.249 g
Crushing	0.5			1.228 g	1.228 g
	0.6			1.228 g	1.165 g
	0.7	1.228 g	0.794 g	1.210 g	1.109 g
	0.8			1.205 g	1.054 g
	0.9			1.152 g	0.953 g
	1.0			1.079 g	0.879 g

in comparison with mainshocks; evaluating the seismic capacity of the RCC building should be conducted using as-recorded seismic sequences.

5.3 Effects of polarity between the mainshock and the aftershock

‘Polarity’ refers to the direction of the aftershock with respect to the mainshock as shown in Fig. 13. Preceding studies show that the polarity of the aftershock with respect to the mainshock is important for cases in which the residual drift after a mainshock is high, and depending on

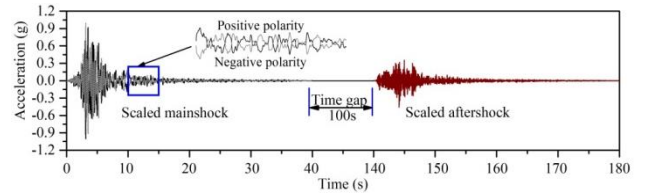


Fig. 13 Two mainshock-aftershock sequences with different mainshock polarities

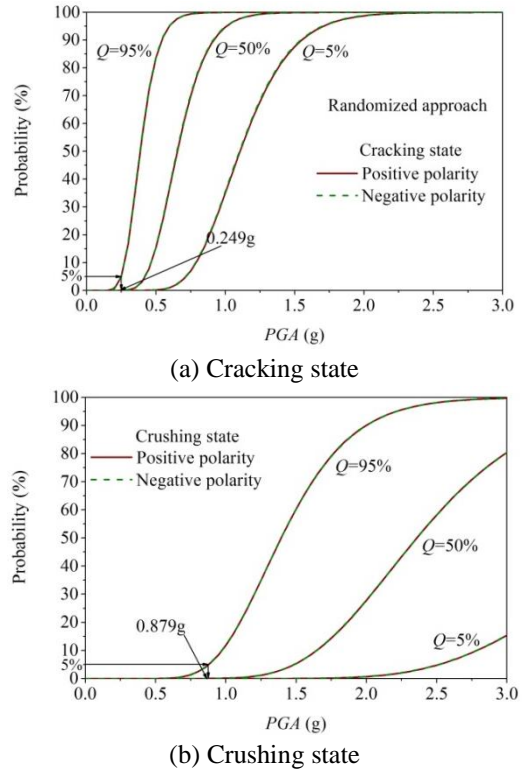


Fig. 14 Fragility curves of the RCC for mainshock-aftershocks considering polarities of mainshocks

the polarity, the aftershock tends to amplify or reduce mainshock residual drift (Luco *et al.* 2004, Raghunandan *et al.* 2015). However, none of the previous studies investigated the residual response of the RCC building after earthquakes and the polarity effect between the mainshock and the aftershock on the RCC is unknown. In this part, the randomized seismic sequences with the PGA_{as}/PGA_{ms} value equal to 1.0 in sect. 5.2 are used to investigate the polarity effect by considering positive and negative polarities of mainshocks. Fragility curves of the RCC building for seismic sequences considering different polarities of mainshocks appear in Fig. 14. It can be clearly seen that fragility curves for different damage states almost overlap, which indicates that the polarity between the mainshock and the aftershock has negligible influence on the probability of cracking or crushing for the RCC model.

6. Conclusions

This paper has summarized the results of an analytical study aimed at providing further understanding on the

influence of aftershocks on seismic performance of a typical RCC building. Three approaches to generate mainshock-aftershock sequences are applied to investigate the effect of mainshock-aftershocks on fragility evaluation of the RCC building, which include the repeated seismic sequence, the randomized seismic sequence, and the as-recorded seismic sequence. Finally, fragility curves are given and HCLPF capacities are determined. The following conclusions are drawn from this investigation:

- The obtained results for as-recorded mainshocks and seismic sequences show that sequential ground motions increase the probability of cracking or crushing for the RCC model significantly in comparison with mainshocks. The HCLPF capacities estimated by only mainshocks would be overestimated in comparison with the corresponding seismic sequences. Specifically, the HCLPF capacity of the RCC building is 0.270 g for the cracking state under mainshocks while has only 0.201 g under seismic sequences, reducing by 25.6 %. For the crushing state, the HCLPF capacity of the RCC building is 1.228 g under mainshocks while the value for seismic sequences has only 0.794 g, with a loss of 35.3 % crushing capacity in comparison with only mainshocks.
- With the increase of the relative intensity of aftershock ground motions, HCLPF capacities of the RCC estimated by artificial seismic sequences, particularly for randomized sequences, decrease considerably. For the PGA_{as}/PGA_{ms} value of 0.5, no difference of the HCLPF capacity for the RCC can be found between mainshocks and both types of artificial seismic sequences. As the PGA_{as}/PGA_{ms} value increases to 1, there is a considerable reduction in HCLPF capacities, with a loss of 3.7 % for cracking capacity and 12.1 % for crushing capacity under repeated sequences, respectively. For randomized sequences, the reduction of HCLPF capacities can reach 7.8 % for cracking state and 28.4 % for crushing state, respectively.
- Repeated seismic sequences lead to the largest HCLPF capacity, which may overestimate the seismic capacity of the RCC building due to the same frequency content between mainshocks and aftershocks. It is recommended that evaluating the seismic capacity of the RCC building should be conducted using as-recorded seismic sequences. If as-recorded seismic sequence is scarce, randomized seismic sequence is a better representative way than repeated seismic sequences.
- The fragility curves for different damage states almost overlap between different polarities of mainshocks. Accordingly, the polarity of the aftershock with respect to the mainshock has no obvious effect on the probability of cracking or crushing for the RCC building.

Indeed, the nuclear power project is a system engineering including complicated interactions between structures and facilities. To emphasize the effect of aftershocks on the evaluation of the RCC building under seismic sequences, a single plant is only considered in this paper. More complex models coupled with foundations, plants, and facilities, and more researches considering the compatibility and adaptability should be conducted in the future.

Acknowledgments

The authors are grateful to the anonymous reviewers for their constructive comments and suggestions. This study is supported by the National Key Research and Development Program of China (2016YFC0701108) and the National Natural Science Foundation of China (No. 51238012, 51322801, 51708161). This support is gratefully acknowledged. Finally, the authors express their gratitude to the two anonymous reviewers that helped to improve the quality of the paper.

References

- ABAQUS Ver. 6.10, Abaqus/CAE User's Manual.
- Alliard, P. and Leger, P. (2008), "Earthquake safety evaluation of gravity dams considering aftershocks and reduced drainage efficiency", *J. Eng. Mech.*, **134**(1), 12-22.
- American Nuclear Society (ANS) (2007), External Events PRA Methodology (ANSI/ANS-58.21-2007), American National Standard, American Nuclear Society, Illinois, USA.
- Campbell, R., Short, S., Ravindra, M., Hardy, M. and Johnson J. (1998), "Seismic reevaluation and upgrading of nuclear power facilities outside the US using US developed methodologies", *Nucl. Eng. Des.*, **181**(1-3), 115-129.
- Cho, S.G. and Joe, Y.H. (2005), "Seismic fragility analyses of nuclear power plant structures based on the recorded earthquake data in Korea", *Nucl. Eng. Des.*, **235**(17), 1867-1874.
- Choi, I.K., Choun, Y.S., Ahn, S.M. and Seo, J.M. (2006), "Seismic fragility analysis of a CANDU type NPP containment building for near-fault ground motions", *KSCE J. Civil Eng.*, **10**(2), 105-112.
- De Grandis, S., Domaneschi, M. and Perotti, F. (2009), "A numerical procedure for computing the fragility of NPP components under random seismic excitation", *Nucl. Eng. Des.*, **239**(11), 2491-2499.
- Efraimiadou, S., Hatzigeorgiou, G.D. and Beskos, D.E. (2013), "Structural pounding between adjacent buildings subjected to strong ground motions, PartII: The effect of multiple earthquakes", *Earthq. Eng. Struct. Dyn.*, **42**(10), 1509-1528.
- Electric Power Research Institute (EPRI) (2003), *Seismic Probabilistic Risk Assessment Implementation Guide* (TR-1002989), EPRI, CA, USA, 2003.
- Ellingwood, B.R. (1998), "Issues related to structural aging in probabilistic risk assessment of nuclear power plants", *Reliab. Eng. Syst. Saf.*, **62**(3), 171-183.
- Faisal, A., Majid, T.A. and Hatzigeorgiou, G.D. (2013), "Investigation of story ductility demands of inelastic concrete frames subjected to repeated earthquakes", *Soil Dyn. Earthq. Eng.*, **44**, 42-53.
- Furukawa, S., Imoto, K., Tanaka, H. and Yoshizaki, S. (1987), "Evaluation method for restoring force characteristics of R/C shear walls of reactor buildings: Part I Evaluation method for restoring force characteristics", *Arch. Inst. JPN*, **1987**, 289-290.
- Ghiocel, D.M., Wilson, P.R., Thomas, G.G. and Stevenson, J.D. (1998), "Seismic response and fragility evaluation for an Eastern US NPP including soil-structure interaction effects", *Reliab. Eng. Syst. Saf.*, **62**(3), 197-214.
- Goda, K. and Taylor, C.A. (2012), "Effects of aftershocks on peak ductility demand due to strong ground motion records from shallow crustal earthquakes", *Earthq. Eng. Struct. Dyn.*, **41**(15), 2311-2330.
- Guneyisi, E.M. and Sahin, N.D. (2014), "Seismic fragility analysis of conventional and viscoelastically damped moment resisting

- frames”, *Earthq. Struct.*, **7**(3), 295-315.
- Han, R.L., Li, Y. and Lindt, J.W. S (2014), “Seismic risk of base-isolated non-ductile reinforced concrete buildings considering uncertainties and mainshock-aftershock sequences”, *Struct. Saf.*, **50**, 39-56.
- Hatzigeorgiou, G.D. (2010a), “Behavior factors for nonlinear structures subjected to multiple near-fault earthquakes”, *Comput. Struct.*, **88**(5-6), 309-321.
- Hatzigeorgiou, G.D. (2010b), “Ductility demand spectra for multiple near-and far-fault earthquakes”, *Soil Dyn. Earthq. Eng.*, **30**(4), 170-183.
- Hatzigeorgiou, G.D. and Beskos, D.E. (2009), “Inelastic displacement ratios for SDOF structures subjected to repeated earthquakes”, *Eng. Struct.*, **31**(11), 2744-2755.
- Hatzigeorgiou, G.D. and Liolios, A.A. (2010), “Nonlinear behavior of RC frames under repeated strong ground motions”, *Soil Dyn. Earthq. Eng.*, **30**(10), 1010-1025.
- Huang, Y.N., Whittaker, A.S. and Luco, N. (2011), “A probabilistic seismic risk assessment procedure for nuclear power plants: (I) Methodology”, *Nucl. Eng. Des.*, **241**(9), 3996-4003.
- Huang, Y.N., Whittaker, A.S. and Luco, N. (2011), “A probabilistic seismic risk assessment procedure for nuclear power plants: (II) application”, *Nucl. Eng. Des.*, **241**(9), 3985-3995.
- Kennedy, R.P. and Ravindra, M.K. (1984), “Seismic fragilities for nuclear power plant risk studies”, *Nucl. Eng. Des.*, **79**(1), 47-68.
- Kim, J.H., Choi, I.K. and Park, J.H. (2011), “Uncertainty analysis of system fragility for seismic safety evaluation of NPP”, *Nucl. Eng. Des.*, **241**(7), 2570-2579.
- Lee, J. and Fenves, G.L. (1998), “Plastic-damage model for cyclic loading of concrete structures”, *J. Eng. Mech.*, **124**(8), 892-900.
- Lee, J. and Kim, J. (2015), “Seismic performance evaluation of moment frames with slit-friction hybrid dampers”, *Earthq. Struct.*, **9**(6), 1291-1311.
- Li, Q. and Ellingwood, B.R. (2007), “Performance evaluation and damage assessment of steel frame buildings under main shock-aftershock sequences”, *Earthq. Eng. Struct. Dyn.*, **36**(3), 405-27.
- Lubliner, J., Oliver, J., Oller, S. and Onate, E. (1989), “A plastic-damage model for concrete”, *Int. J. Solid. Struct.*, **25**(3), 299-326.
- Luco, N., Bazzurro, P. and Cornell, C.A. (2004), “Dynamic versus static computation of the residual capacity of a mainshock-damaged building to withstand an aftershock”, *Proceedings of the 13th World Conference on Earthquake Engineering*, Vancouver, Canada, August.
- Mazzoni, S., McKenna, F., Scott, M.H. and Fenves, G. (2004), *OpenSees Users Manual*, PEER, University of California, Berkeley.
- Nakamura, N., Akita, S., Suzuki, T., Koba, M., Nakamura, S. and Nakano, T. (2010), “Study of ultimate seismic response and fragility evaluation of nuclear power building using nonlinear three-dimensional finite element model”, *Nucl. Eng. Des.*, **240**(1), 166-180.
- Olmos, B.A., Jara, J.M. and Jara, M. (2012), “Influence of some relevant parameters in the seismic vulnerability of RC bridges”, *Earthq. Struct.*, **3**(3-4), 365-381.
- Ozaki, M., Okazaki, A., Tomomoto, K., Iba, T., Satoh, R., Nanba, H., ... and Ugata, T. (1998), “Improved response factor methods for seismic fragility of reactor building”, *Nucl. Eng. Des.*, **185**(2), 277-291.
- Park, Y.J. and Hofmayer, C.H. (1994), *Technical Guidelines for Aseismic Design of Nuclear Power Plants*, Nuclear Regulatory Commission, Washington, DC, United States.
- Park, Y.J., Hofmayer, C.H. and Chokshi, N.C. (1998), “Survey of seismic fragilities used in PRA studies of nuclear power plants”, *Reliab. Eng. Syst. Saf.*, **62**(3), 185-195.
- PEER Strong Motion Database, <http://peer.berkeley.edu>.
- Raghunandan, M., Liel, A.B. and Luco, N. (2015), “Aftershock collapse vulnerability assessment of reinforced concrete frame structures”, *Earthq. Eng. Struct. Dyn.*, **44**(3), 419-439.
- Ranjbaran, F. and Hosseini, M. (2014), “Seismic vulnerability assessment of confined masonry wall buildings”, *Earthq. Struct.*, **7**(2), 201-216.
- Ruiz-García, J. and Negrete-Manriquez, J.C. (2011), “Evaluation of drift demands in existing steel frames under as-recorded far-field and near-fault mainshock-aftershock seismic sequences”, *Eng. Struct.*, **33**(2), 621-634.
- Shin, J., Kim, J.H. and Lee, K. (2014), “Seismic assessment of damaged piloti-type RC building subjected to successive earthquake”, *Earthq. Eng. Struct. Dyn.*, **43**(11), 1603-1619.
- Takeda, M., Ohkawa, Y. and Akutsu, Y. (1998), “An evaluation method for seismic isolation effect in siting of a nuclear facility”, *Reliab. Eng. Syst. Saf.*, **62**(3), 241-249.
- Tesfamariam, S., Goda, K. and Mondal, G. (2014), “Seismic vulnerability of RC frame with unreinforced masonry infill due to mainshock-aftershock earthquake sequences”, *Earthq. Spectra*, **31**, 1427-1449.
- U.S. Nuclear Regulatory Commission (USNRC) (1983), *PRA Procedures Guide* (NUREG/CR-2300), U.S. Nuclear Regulatory Commission, Washington, DC, United States.
- Vamvatsikos, D. and Cornell, A.C. (2002), “Incremental dynamic analysis”, *Earthq. Eng. Struct. Dyn.*, **31**(3), 491-514.
- Vermaut, M., Monette, P., Shah, P. and Campbell, R.D. (1998), “Methodology and results of the Seismic Probabilistic Safety Assessment of Krško nuclear power plant”, *Nucl. Eng. Des.*, **182**(1), 59-72.
- Viallet, E., Labbé, P., Gallitree, E., Nadjarian, A., Vandeputte, D., Ravet, S., ... and Pons, Y. (2010), “Seismic re-evaluation of EDF Bugey 900 PWR nuclear power plant in the frame of the 3rd periodic safety review”, *Nucl. Eng. Des.*, **240**(6), 1306-1319.
- Zentner, I. (2010), “Numerical computation of fragility curves for NPP equipment”, *Nucl. Eng. Des.*, **240**(6), 1614-1621.
- Zhai, C.H., Wen, W.P., Li, S., Chen, Z. and Xie, L.L. (2014), “The damage investigation of inelastic SDOF structure under the mainshock-aftershock sequence-type ground motions”, *Soil Dyn. Earthq. Eng.*, **59**, 30-41.
- Zhai, C.H., Zheng, Z., Li, S. and Xie, L.L. (2015), “Seismic analyses of a RCC building under mainshock-aftershock seismic sequences”, *Soil Dyn. Earthq. Eng.*, **74**, 46-55.
- Zhang, S.R., Wang, G.H. and Sa, W.Q. (2013), “Damage evaluation of concrete gravity dams under mainshock-aftershock seismic sequences”, *Soil Dyn. Earthq. Eng.*, **50**, 16-27.